Vortex-Induced Vibrations of a Circular Cylinder at Low Reynolds Numbers

Minhyung Lee*, Sung-Yeoul Lee
School of Mechanical and Aerospace Engineering, Sejong University, Seoul 143-747, Korea

The vortex-induced vibrations of a circular cylinder at low Reynolds (Re) numbers are simulated by applying a method of the two-dimensional computational fluid dynamics coupled with the structural dynamics based on the multi-physics. The fluid solver is first tested on the case of a fixed cylinder at $Re \leq 160$, and shows a good agreement with the previous high-resolution numerical results. The present study then reports on the detailed findings concerning the vibrations of an elastic cylinder with two degrees of translational freedom for a number of cases in which Re is fixed at 200, a reduced damping parameter $Sg=0.01$, 0.1, 1.0, 10.0 and the mass ratio $M^*=1$, 10.

Key Words: Vortex-Induced Vibrations, A Circular Cylinder, Multi-Physics

1. Introduction

All structures under the influence of fluid can experience deformation under static or dynamic loads. When the deformation is caused by fluid around a structure, it causes changes in dynamic load, which leads to further deformation and so on. This is because the fluid flow depends on the geometry of the structure and the orientation of the various structural components. These interactions can develop into complicated vibrations of the structure and eventually, structural damage may occur under to certain unfavourable conditions. Parkinson (1989) provided some comprehensive reviews on the fluid-structure interaction problems. Among problems associated with fluid-structure interactions, the vortex-induced vibration of a circular cylinder has drawn attention for many years due to its strong vortex shedding. For example, it can cause vibrations in heat exchanger tubes, it is important to the design of civil structures such as bridges, as well as the design of ocean structures. The practical significance of vortex-induced vibration has led to numerical (Williamson, 1996) and experimental studies (West and Apelt, 1997), many of which have initially concentrated on rigid structures in a cross flow, and have then progressed into elastic structures because of their growing importance in many engineering fields.

It is known that the cross flow vibration amplitude has a strong relationship with the phase difference between the lift force and the cylinder motion (Zhou et al., 1999). As Griffin (1992) derived from a series of data, the vibration amplitude depends on a reduced damping parameter, $Sg=8\pi^2 St^2 \alpha M^*$. Here, $St=f_s D/U_\infty$ is the Strouhal number, $M^*=m/\rho D^2$ the mass ratio, α the damping factor in the structural dynamics equations, D the cylinder diameter, U_∞ the undisturbed freestream velocity, f_s the vortex shedding frequency, m the mass per unit length of the cylinder, and ρ the fluid density.

Although there is a need to improve our knowledge of the basic flow phenomena and the interrelated structural behaviours as well, much less numerical work has been carried out due to the

* Corresponding Author,
E-mail : mlee@sejong.ac.kr
TEL : +82-2-3408-3282; **FAX** : +82-2-3408-3333
School of Mechanical and Aerospace Engineering, Sejong University Seoul, 143-747 Korea. (Manuscript **Received** October 19, 2002; **Revised** July 28, 2003)

complex multi-physics associated with the problems. In recent years, however, substantial progress has been made in the development of an improved understanding of unsteady fluid dynamics and structural dynamics. The computational methods for unsteady fluid dynamics have been developed based on Eulerian Navier-Stokes formulation of fluid dynamic equations in the time domain. On the other hand, the structural side of computational methods has evolved by using the finite element method based on the Lagrangian formulation. Since these methods are firmly established and widely used in practice, it is wise to take full advantage of the developments in both fields by coupling the fluid and structural solvers. This partitioned analysis for fluid structure interaction provides an efficient and modular way to deal with fluid-structure interaction problems treated in the current study.

Slaouti and Stansby (1994) analysed the force and free vibration of a flexible circular cylinder using the vortex-in-cell (VIC) method. Their analysis was carried out for a fixed value of Sg and M^*. For the free vibration case, only the time history results of the lift and drag coefficients are provided. More recently, Zhou et al.(1999) also studied the vortex induced vibrations of an elastic circular cylinder with two-degrees of freedom using the same VIC discrete vortex method (Graham, 1988). In the present approach, the code is structured in such a manner that the fluid and the structure solvers can be modelled separately by using the domain decomposition approach, so that the interaction between the fluid and the structure can be properly accounted for. In this paper, an in-depth analysis of the effect of vortex shedding behind the cylinder on the vibrations of an elastic cylinder is provided. The present work focuses on the development of the analysis method for the fluid-structure interactions rather than on the enhancement of the fluid solver.

2. Numerical Approach

The flow analysis and the structural response are coupled in the time marching process. The instantaneous values of forces from the unsteady flow solution are used in a simultaneous solution of the structural solution. As an implicit system needs to be solved iteratively at each time step for the flow equations, the structure equations can be coupled fully with the flow equation without ony time delay.

2.1 Fluid model

The physical problem under consideration is that of incompressible viscous flow and the mathematical model used is the two-dimensional Navier-Stokes equations. The equations governing the flow field are continuity and momentum equations. When the computational domain moves as a function of time, the grid velocity v_g is involved and should be included in discretizing the governing equations. The integral form of the governing equations can be written as,

$$\frac{d}{dt}\int_{\Omega}\rho d\Omega+\int_{s}\rho(v-v_g)\cdot nds=0 \tag{1}$$

$$\frac{d}{dt}\int_{\Omega}\rho\phi d\Omega+\int_{s}\rho\phi(v-v_g)\cdot nds=\int_{s}\gamma\nabla\phi\cdot nds+\int_{\Omega}q_{\phi}d\Omega \tag{2}$$

where Ω is an arbitrary moving volume and S is the surface area. ϕ represents the conserved property per unit mass, and $\gamma\nabla\phi$ and q_{ϕ} are the diffusive flux and source terms, respectively.

When the control volume moves, the space conservation law (SCL) has to be satisfied. This law relates the rate of change of CV volume with its surface velocity and expressed as,

$$\frac{d}{dt}\int_{\Omega}dV-\int_{s}v_g\cdot ndS=0 \tag{3}$$

The equations are solved by using the finite volume (FV) method, and the solution domain has been divided into a finite number of control volumes (CV) that can be of any shape.

The process of numerical analysis begins with discretization of the differential equations that results in algebraic equations. The effective discretization method is required to reduce the errors associated with it. In this study, the central difference scheme (CDS) which is one of the linear

interpolation methods is used. The midpoint rule is used to approximate of both the surface and volume integrals. The unknown integrands of the convective and diffusive terms at the cell-face centre have to be interpolated from the CV centre. Therefore, interpolation and numerical differentiation have to be used to express the cell-face values of variables and their derivatives through the nodal values. The cell-face values of the variables are approximated by using a linear interpolation given by

$$\phi_e \approx \phi_{e'} = \phi_E \lambda_e + \phi_P (1-\lambda_e) \tag{4}$$

where the linear interpolation factor λ_e is defined as,

$$\lambda_e = \frac{x_e - x_P}{x_E - x_P} \tag{5}$$

Subscripts e, P and E represent the midpoint of east cell-face, CV centre node and CV centre node of east cell, respectively. Eq. (3) is a second-order approximation at mid-point location. However, in the case of non-uniform mesh, the mid-point may lay off some position, and the second-order accuracy cannot be achieved. Thus, the grid quality can be analysed by comparing position vectors of the mid-point and cell-faces. The second-order accuracy can be restored by adding a correction term as follows,

$$\phi_e \approx \phi_{e'} + (\nabla \phi)_{e'} \cdot (r_e - r_{e'}) \tag{6}$$

where r_e and $r_{e'}$ are the position vectors. The use of the CDS is widely accepted due to its simplicity with reasonable accuracy. The main cause of the truncation error is more closely associated with the mesh density.

The established SIMPLE algorithm is used to solve the pressure-velocity coupling. This is a time-marching procedure that starts the process with a guessed pressure field. The linearized momentum equations are solved in each time step, and the mass conservation is imposed on the new velocities by applying a velocity correction that is related to the gradient of the pressure correction.

2.2 Structural model

Two-dimensional structural model is developed to simulate the motion of the elastic cylinder under dynamic loading. It is assumed that the circular cylinder is mounted as a spring-mass-damper system, which represents the situation at a section of a long cylindrical structure at the location of the maximum amplitude of the vibration. The equations of motion for the cylinder displacement can be expressed as,

$$\frac{d^2\chi}{dt^2} + 2a\omega_n \frac{d\chi}{dt} + \omega_n^2 \chi = \frac{F(t)}{m} \tag{7}$$

where $\omega_n = \sqrt{k/m} = 2\pi f_n$ is the angular natural frequency of cylinder, f_n the natural frequency of the cylinder, $\chi = X\mathbf{i} + Y\mathbf{j}$, X and Y are the instantaneous displacements of the cylinder in the x- and y-directions, respectively, k the rigidity of the cylinder, and $F(t)$ the induced force. Dimensionless form of the equation of motion respect to the cylinder diameter can be written as

$$\frac{d^2\bar{\chi}}{d\tau^2} + 4a\pi St^* \frac{f_n}{f_s^*} \frac{d\bar{\chi}}{d\tau} + \left(2\pi St^* \frac{f_n}{f_s^*}\right) \bar{\chi} = \frac{C_f}{2M^*} \tag{8}$$

where $\bar{\chi} = \chi/D$, $\tau = tU_\infty/D$, and f_s^* is the vortex-shedding frequency of the rigid cylinder. Note that the Strouhal number St^* is obtained for the rigid cylinder. The applied force coefficient is $C_f = 2F(t)/\rho D U_\infty^2$.

The force on the cylinder is calculated by integrating the pressure and the wall shear stress around the cylinder surface. For the total force $F = F_x\mathbf{i} + F_y\mathbf{j}$, as shown in Fig. 1, the drag and lift coefficients are given by

$$C_d = \frac{2F_x}{\rho D U_\infty^2} \text{ and } C_l = \frac{2F_y}{\rho D U_\infty^2} \tag{9}$$

The equations of motion can then be solved with

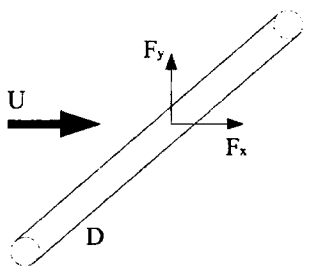

Fig. 1 Loading lift and drag forces

a numerical integration scheme. In the present analysis, the direct integration method based on linear variation of acceleration is employed to find the dynamic responses of the system in the time domain. The response solution is obtained by using a step-by-step time integration finite difference approach. This method is conditionally stable. A Domain decomposition approach is applied for the coupling of the fluids and structures. The data that need to be transfered for this approach are dynamic loads and position of the elastic cylinder. The mutual time step is determined from the stability requirements of both the fluid and the structure. The implied time step restriction on the structure scheme is implied: $\Delta t_{crit} = T_n/\pi$, where T_n is the smallest natural time of period. In our calculations, the largest frequency considered is $2\pi St^*(f_n/f_s^*) = (2.0 \times 3.1415 \times 0.185 \times 5.02) = 5.83$. The shortest period is $1/5.83 = 0.171$. Hence, the critical time step is $0.171/\pi = 0.055$. On the other hand, the convergence of the fluid solver for the cortex-shedding frequencies was obtained at $dtU_\infty/D < 0.03 = \tau < 0.03$ (Park et al., 1998). The time step required to obtain accurate results for structural response solution was in general found to be larger than the maximum time step needed for the flow solver. Therefore, the time step selected is drawn from the critical time step of the fluid solver.

3. Results

3.1 Rigid cylinder

In order to verify the ability of the numerical computation to accurately resolve unsteady flow and its associated phenomena such as vortex shedding, the flow past a fixed circular cylinder is analysed first. The computational domain used is $-50D < x < 50D$ and $-50D < y < 50D$, where the origin corresponds to the centre of the cylinder. As shown in Fig. 2, the grid size of 313×169 is created with O-mesh generation and 313 points are placed on the cylinder surface for sufficient resolution of the flow pattern close to the cylinder. Six test cases are examined out at $Re < 200$. For all cases investigated in this study, the time step $\Delta tU_\infty/D$ was set to 0.02. About 5 iterations per time step were required for convergence. The calculation usually took 44 hours on a 2 GHz personal computer (PC).

Figure 3 shows the Strouhal number versus the Reynolds number. The calculated Strouhal number is compared with the correlated equation (Williamson, 1998) and the numerical results (Park et al., 1998). The number of grid used (Park et al., 1998) was 641×241, which is about three times that of the current grid number. The results are in good agreement, although some discrepancy due to the grid density has been observed at low Re. As shown in Table 1, comparison of the force coefficients obtained from several sources also shows discrepancies (Bearman,

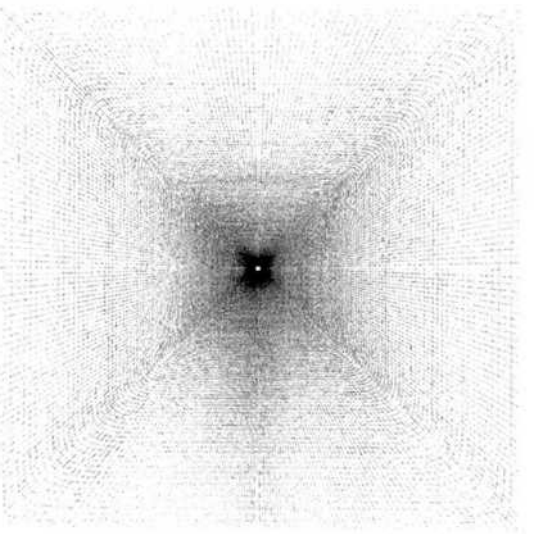

Fig. 2 Grid size of 313×169 with O-mesh generation

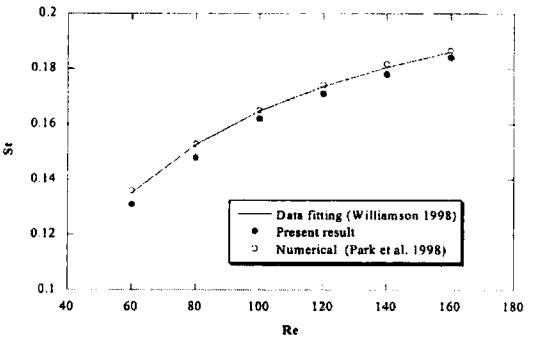

Fig. 3 Strouhal number vs. Reynolds number

Table 1 Drag and lift coefficients at Re=100, Bearman (1998)

Source	$C_{D\,mean}$	$C_{L\,rms}$
Arkell & Graham Discrete vortex	1.33	0.17
Beaudan & Moin High order finite diff.	1.35	0.24
Chaplin Spectral-differenec	1.29	0.20
Gushchin Finite difference	1.38	n/a
Karniadakis Spectral-element	1.42	0.26
Kravchenko Galerkin B-spline	n/a	0.23
Mittal Spectral method	n/a	0.23
Savvides Spectral-difference	1.30	0.16
Savvides Spectral-element	1.32	0.14
Sherwin Spectral-element	1.36	0.24
Younis Finite difference	1.46	0.34
Present Calculation	1.326	0.22

1998). A set of 12 numerically simulated force coefficients at Re=100, are compared and the variation of $C_{d\,mean}$ and $C_{l\,rms}$ were found to be 1.30~1.46 and 0.14~0.34. This indicates that a completely converged solution for the current problem at hand has not been achieved yet. From the test on the grid density, the cross-spanwise direction grid refinement is found to have greater influence than that of the spanwise direction. However, the present study provides a reasonably accurate results and demonstraties that the flow solver is adequete for to be use in simulation of the elastic cylinder.

A rigid cylinder with Re=200 is simulated again because the flow is essentially laminar (Slaouti and Stanby, 1992) and three-dimensional wake transition develops for Re from 190 up to 260 (Williamson, 1996). Figures 4 and 5 show the time histories of the lift and drag coefficients and the vortex pattern, respectively. In Fig. 4, the lift and drag force coefficients settle into a sinusoidal periodic function after the formation of wake instability leading to vortex shedding with a mean value of around 1.318 for the drag coefficient. In Fig. 5, the vortex pattern in the wake at the dimensionless time $\tau=150$ shows the well-known Karman vortex street. The Strouhal number for the rigid cylinder, St^* and the

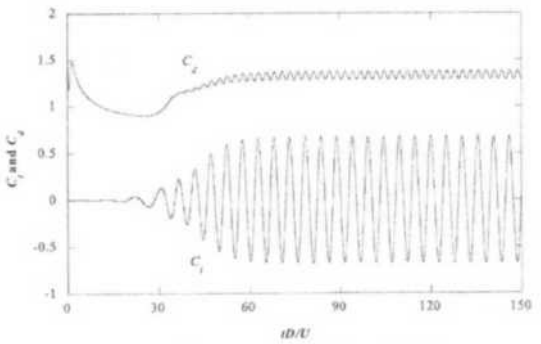

Fig. 4 Force coefficients time histories for a rigid cylinder at Re=200

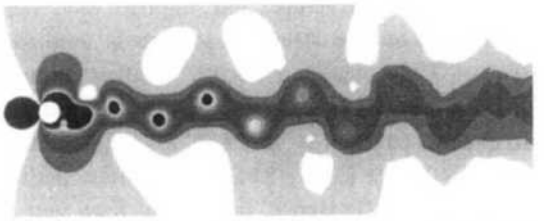

Fig. 5 The pressure distribution in the wake, Re=200

mean value of C_d are found to be 0.1928 and 1.318. These St^* and $C_{d\,mean}$ are in excellent agreement with the numerical results (Zhou et al., 1999) of $St^*=0.1922$ and $C_{d\,mean}=1.32$. Therefore, all the expected features of a rigid cylinder in a cross-flow are correctly described by the proposed method.

3.2 Elastic cylinder with Re=200

Simulations of the elastic cylinder is carried out by adopting two-degrees of translational freedom of the structural model for Re=200. The test parameters were the mass ratio M^*, the reduced damping Sg and the frequency ratio f_n/f_s^*. The mass ratio M^* is set to 1.0 or 10.0, while Sg varies from 0.01 to 10.0. These parameters are chosen because some experimental and computational data are available for comparison. Figure 6 shows the maximum cylinder vibration amplitude versus Sg at $M^*=1.0$, which is known as the Griffin plot of peak-amplitude. The simulation results were also plotted with previous experimental data. The extensive amount of data obtained both in air and in water was compiled by Griffin (1980) from

numerous experimentd investigations. We have chosen to replot the data using a linear vertical axis. This is because the experimental data reveals a large scatter in the amplitude, which is not evident in the classical log-log plots. The simulation results can predict the attenuation of the vibration amplitude as the damping parameter Sg guite well. Although it seems that the simulations slightly overpredict the cylinder vibration amplitude for higher values of mass damping, generally a good correlation is attained.

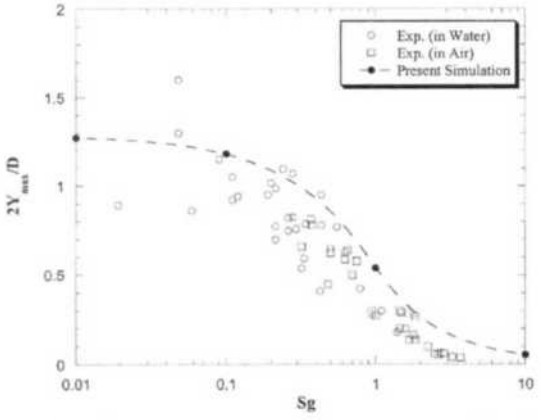

Fig. 6 Flow-induced cross flow vibration amplitude versus Sg. Re=200 and $M^*=1.0$, experimental data (○, □) from Griffin (1992)

Figure 7 shows the X-Y phase plots for Sg= 0.01, 0.1, 1.0 and 10.0. It clearly shows the cylinder response is a self limiting oscillation with a pattern also shown in Figure 8. An increase in Sg from 0.01 to 0.1 has little effect on the vibration amplitude but a further increase in Sg to 10.0 from 1.0 creates a sharp drop in the amplitude as predicted in the Griffin plot. The Figure 8 pattern exists in all cases in which the amplitude decreuae as Sg increases and the equilibrium position of the cylinder in the streamwise direction is no longer at zero due to the mean drag force. This position also varies as the value of Sg changes.

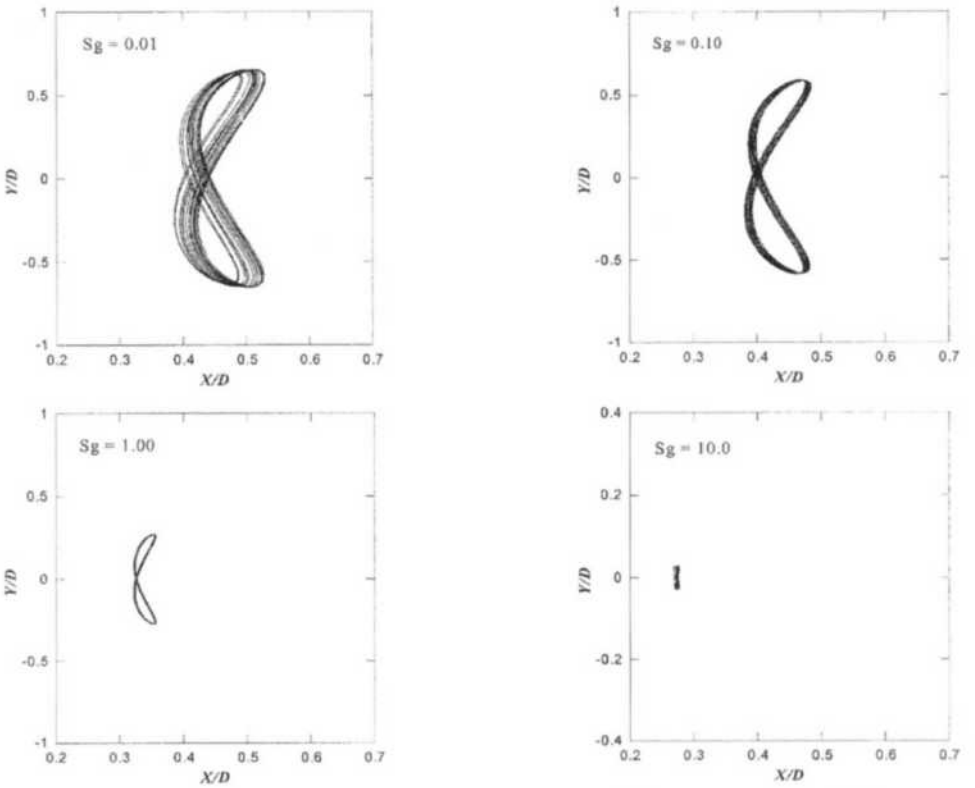

Fig. 7 X-Y phase plot for the case with Re=200, $M^*=1.0$ and $f_m/f_s^*=1.30$

Figure 8 shows the time histories of the drag and lift coefficients together with the cross-flow displacement of the cylinder for Sg=0.01 and $M^*=1.0$. In order to have a clear picture of vortex induced response, the frequency ratio f_n/f_s^* is chosen to vary from 0.65 to 5.20 but most values is concentrated around $f_n/f_s^*=1$ as this region was expected to have significant flow structure interactions. It can be observed that the time histories of the force coefficients are similar to that of the rigid case as the frequency ratio f_n/f_s^* increases. For the case of $f_n/f_s^*=5.20$, there was almost no oscillation in both directions as the equilibrium position in the streamwise direction is about 0.017 and the maximum amplitude of the cross-flow direction is about 0.009. In other words, the elastic cylinder displaces less oscillatory movement as the stiffness of structure increases, as expected. The equilibrium position in the streamwise direction is varied from $X/D=1.05$ for $f_n/f_s^*=0.65$ through $X/D=0.55$ for $f_n/f_s^*=1.16$ to $X/D=0.017$ for $f_n/f_s^*=5.2$. However, the maximum amplitude of oscillation was around 0.1 i.e., around 1/10 of the maximum amplitude in the cross flow direction, and the mean drag increases with increase in the amplitude. These oscillations in both directions for the flexible cases indicate that the vortex structure in the wake experiences dramatic changes in flow compare with the rigid or less flexible cylinder cases. The beating pattern appearing at $f_n/f_s^*=1.73$ has two distinctive frequencies, and this clearly shows the significance of the elastic effect, as shown in the figure. It is also interesting to note that the phase between the lift force and the displacement changes from the 'out-of-pahse' to 'in-phase' mode as the frequency ratio f_n/f_s^* varies from smaller than 0.87 to greaterthan 0.87.

The time histories of the drag and lift coefficients together with the cross-flow displacement of the cylinder for Sg=1.0 with $M^*=1.0$ is shown in Fig. 9. It can be seen that the amplitude of

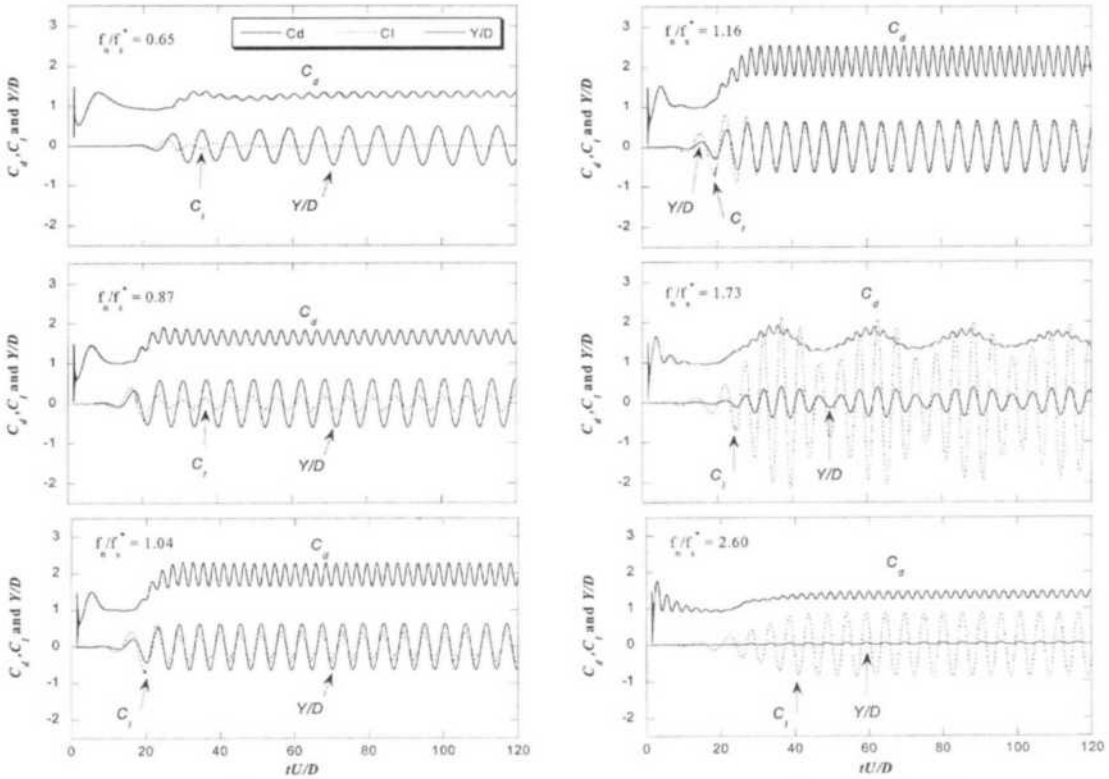

Fig. 8 Forces and displacement time histories, Re=200, Sg=0.01 and $M^*=1.0$

the response and the equilibrium position in the streamwise direction decrease as Sg and M^* values are increased and the beating pattern observed for lower Sg values disappears. These behaviors are expected as the increase in Sg and M^* effectively increases the damping and reduces the applied load on the cylinder structure. Also to be noticed is that the phase shift pattern changes case by case. However the out-of-phase pattern occurs at lower values of f_n/f_s^* and vise versa at higher values.

Figures 10, 11, 12 and 13 show the results of the mean drag coefficient $C_{d\,\mathrm{mean}}$, the root mean square values of the lift coefficient $C_{l\,\mathrm{rms}}$, the root mean square values of the y-displacement, and the vortex shedding frequency ratio f_s/f_s^* versus

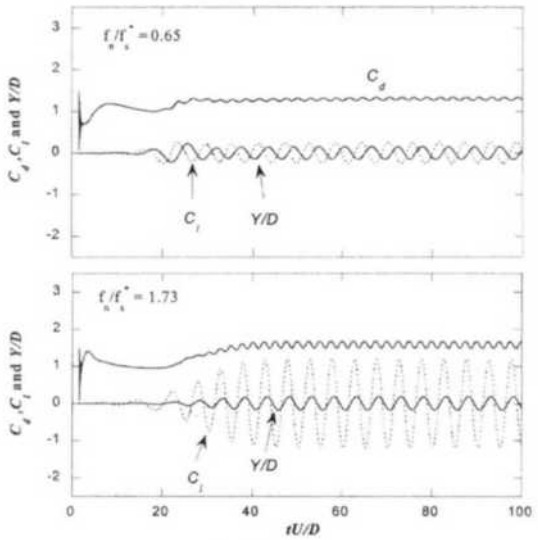

Fig. 9 Forces and displacement time histories, Re=200, Sg=1.0 and $M^*=1.0$

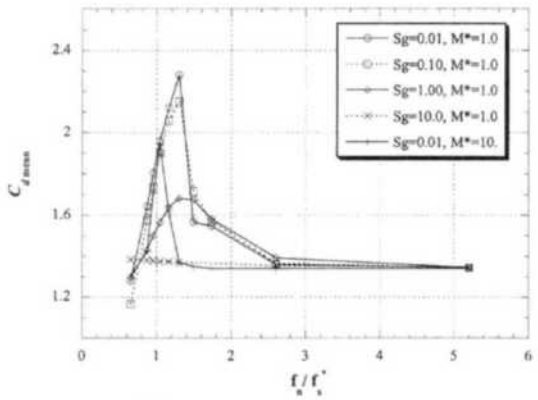

Fig. 10 Variation of mean C_d with f_n/f_s^*

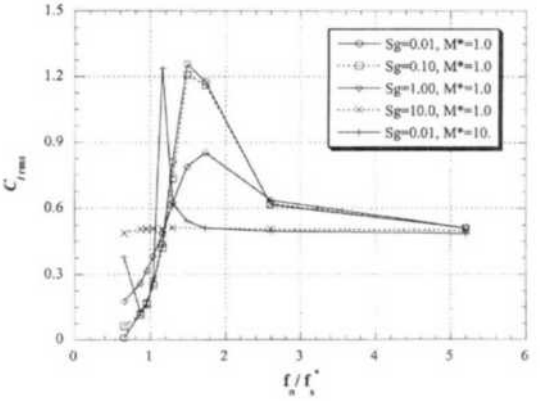

Fig. 11 Variation of $C_{l\,\mathrm{rms}}$ with f_n/f_s^*

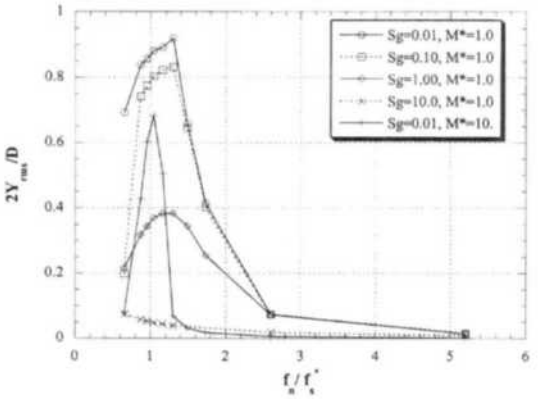

Fig. 12 Variation of $2Y_{\mathrm{rms}}/D$ with f_n/f_s^*

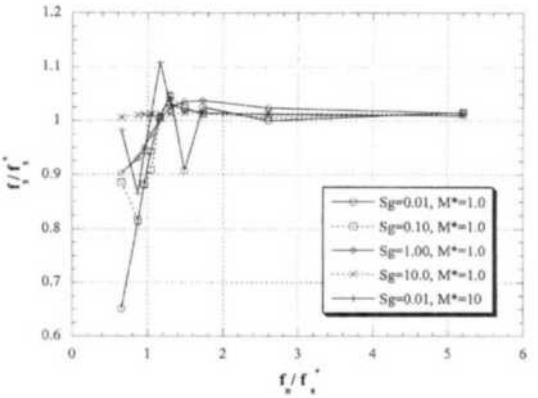

Fig. 13 Variation of vortex-shedding frequency with f_n/f_s^*

f_n/f_s^*, respectively. The mean drag coefficient and the root mean square values of the lift coefficient for $M^*=1$ reach their maximum value at the frequency ratios of $f_n/f_s^* \approx 1.3$ and 1.49, respectively. Then these parametric values are converge into those for the rigid cylinder case as the frequency ratio f_n/f_s^* increases. For the $M^*=10$ case, the maximum values for $C_{d\,\mathrm{mean}}$ and $C_{l\,\mathrm{rms}}$ occur at $f_n/f_s^* \approx 1.04$ and 1.16, respectively. In general, the most excited vibration would be expected to occur when the vibration frequency of the structure is close to the natural frequency of the fluid.

4. Conclusions

The vortex-induced vibrations of an elastic circular cylinder are investigated with the unsteady incompressible Navier-Stokes solver coupled with the structural dynamics code using the multi-physics approach. The results for a fixed cylinder are showed an encouraging consistency with the previous high-resolution results obtained by Park et al.(1998). Based on this validation, an elastic cylinder case is simulated with a two-degrees-of-translational-freedom in structural model. The elastic cylinder cases are investigated with Re=200 as this retains the features of the laminar flow and the two-dimensional feature in the wake. The response of the cylinder, the induced forces, the vortex-shedding frequency and the vortex structure in the wake are examined in detail.

The amplitude of the transverse (cross flow) vibration can be as high as $0.6D$ for the cases considered the current study. The mean drag force also increases substantially compared to the fixed cylinder case. The limit cycle oscillation of the cylinder is clearly captured and the interaction between the fluid and the structure is examined. It is also observed that the vibration depends strongly on the reduced damping parameter Sg and the mass ratio M^*.

Acknowledgment

This work has been supported in part by EESRI(02-006), which is funded by MOCIE (Ministry of Commerce, Industry and Energy).

References

Bearmann, P., 1998, "Development in the Understanding of Bluff Body Flows," *JSME International Journal, Series* B, Vol. 4, No. 1, pp. 103~114.

Graham, J. M. R., 1988, "Computation of Viscous Separated Flow Using a Particle Method," in *Numerical Methods in Fluid Mechanics*, Vol. 3, pp. 310~317, Oxford University Press.

Griffin, O. M., 1992, "Vortex-Induced Vibrations of Marine Structures in Uniform and Sheared Currents," NSF Workshop on Riser Dynamics, University of Michigan.

Griffin, O. M., 1980, "Vortex-Excited Cross-Flow Vibrations of a Single Cylindrical Tube," *ASME Journal of Pressure Vessel Technology*, Vol. 102, pp. 158~166.

Park, J., Kwon, K. and Choi, H., 1998, "Numerical Solutions of Flow Past a Circular Cylinder at Reynolds Numbers up to 160," *KSME Int. Journal*, Vol. 12, No. 6, pp. 1200~1205.

Parkinson, G., 1989, "Phenomena and Modeling of Flow-Induced Vibrations of Bluff Bodies," *Progress in Aerospace Science*, Vol. 26, pp. 169~224.

Slaouti, A. and Stansby, P. K., 1992, "Flow Around Two Circular Cylinders by the Random-Vortex Method," *Journal of Fluids and Structures*, Vol. 6, pp. 641~670.

Slaouti, A. and Stansby, P. K., 1994, "Forced Oscillation and Dynamics Response of a Cylinder in a Current Investigation by the Vortex Method," Proceedings BOSS '94 Conference MIT, pp. 645~654.

West, G. S. and Apelt, C. J., 1997, "Fluctuating Lift and Drag Forces on Finite Lengths of a Circular Cylinder in the Subcritical Reynolds Number Range," *Journal of Fluids and Structures*, Vol. 11, pp. 135~158.

Williamson, C. H. K., 1996, "Vortex Dynamics in the Cylinder Wake," *Annual Review of Fluid Dynamics*, Vol. 28, pp. 477~539.

Williamson, C. H. K. and Brown, G. L., 1998,

"A Series in 1/Re to Represent the Strouhal-Reynolds Number Relationship of the Cylinder Wake," *Journal of Fluids and Structures*, Vol. 12, pp. 1073~1085.

Zhou, C. Y., So, R. M. C. and Lam. K., 1999, "Vortex-Induced Vibrations of an Elastic Circular Cylinder," *Journal of Fluids and Structures*, Vol. 13, pp. 165~189.